Combined electrical transport and capacitance spectroscopy of a MoS2-LiNbO3 field effect transistor

Wladislaw Michailow, Florian J. R. Schülein, Benjamin Möller, Edwin Preciado, Ariana E. Nguyen, Gretel von Son, John Mann, Andreas L. Hörner, Achim Wixforth, Ludwig Bartels, Hubert J. Krenner

Combined electrical transport and capacitance spectroscopy of a MoS$_2$-LiNbO$_3$ field effect transistor

Wladislaw Michailow, Florian J. R. Schülein, Benjamin Möller, Edwin Preciado, Ariana E. Nguyen, Gretel von Son, John Mann (iD), Andreas L. Hörner, Achim Wixforth (iD), Ludwig Bartels, and Hubert J. Krenner (iD)

View Online   Export Citation   CrossMark

ARTICLES YOU MAY BE INTERESTED IN

Combined electrical transport and capacitance spectroscopy of a MoS₂-LiNbO₃ field effect transistor

Wladislaw Michailow,[1,a] Florian J. R. Schülein,[1,2] Benjamin Möller,[1] Edwin Preciado,[3] Ariana E. Nguyen,[3] Gretel von Son,[3] John Mann,[4] Andreas L. Hörner,[1] Achim Wixforth,[1,2] Ludwig Bartels,[3] and Hubert J. Krenner[1,2,b]

[1]*Lehrstuhl für Experimentalphysik 1 and Augsburg Centre for Innovative Technologies (ACIT), Universität Augsburg, Universitätsstr. 1, 86159 Augsburg, Germany*
[2]*Nanosystems Initiative Munich (NIM), Schellingstr. 4, 80799 München, Germany*
[3]*Chemistry Department and Materials Science & Engineering Program, University of California, Riverside, California 92521, USA*
[4]*Department of Physics, Pepperdine University, Malibu, California 90263, USA*

We have measured both the current-voltage (I_{SD}-V_{GS}) and capacitance-voltage (C-V_{GS}) characteristics of a MoS₂-LiNbO₃ field effect transistor. From the measured capacitance, we calculate the electron surface density and show that its gate voltage dependence follows the theoretical prediction resulting from the two-dimensional free electron model. This model allows us to fit the measured I_{SD}-V_{GS} characteristics over the *entire range* of V_{GS}. Combining this experimental result with the measured current-voltage characteristics, we determine the field effect mobility as a function of gate voltage. We show that for our device, this improved combined approach yields significantly smaller values (more than a factor of 4) of the electron mobility than the conventional analysis of the current-voltage characteristics only. *Published by AIP Publishing.*
[http://dx.doi.org/10.1063/1.4973862]

After the rise of graphene,[1–3] a wide range of two-dimensional (2D) materials[4] shifted into the focus of fundamental and applied research.[5] One particularly important class of 2D materials is transition metal dichalcogenides (TMDs).[6] One important representative TMD is molybdenum disulfide, MoS₂, whose indirect band gap changes to a direct one when its thickness is reduced to one single monolayer.[7,8] The resulting high optical activity and sizable bandgap of ~1.9 eV make this material ideally suited for optoelectronic applications,[9] and thus, the optical and electronic properties of MoS₂ and related materials have been investigated intensively in recent years.[10] In particular, field effect transistors (FETs) and logical circuit prototypes have been devised and realized.[11–13] In such devices, source and drain contacts are patterned onto the TMD film, and the charge carrier density is controlled by gate contacts. For FET devices, the transport mobility of the charge carriers in the conducting channel is of paramount importance. Here, different approaches exist to derive this key figure for FET devices. The most commonly applied method is to measure the source-drain current I_{SD} as a function of the gate voltage V_{GS}. Then, the field effect mobility μ_{FE} is determined from a tangent to the linear region of the $I_{SD}(V_{GS})$-dependence using the following formula known from the FET theory

$$\mu_{FE} = \frac{\partial I_{SD}}{\partial V_{GS}} \cdot \frac{A}{C(V_{GS})} \cdot \frac{L}{w} \cdot \frac{1}{V_{SD}}. \quad (1)$$

Here, $C(V_{GS})/A$ is the capacitance per unit area, V_{SD} the source-drain voltage, $\frac{\partial I_{SD}}{\partial V_{GS}}$ the slope of the linear region, L the

length, and w the width of the conducting channel. The intersection of the tangent with the abscissa represents the threshold voltage, V_{Th}. However, this simple FET formula (1) assumes that the mobility is independent of the gate voltage. Moreover, the underlying parallel-plate capacitor model used to quantify the capacitance[11,14] assumes perfectly conducting, infinitely large plates. These assumptions may represent an oversimplification for 2D semiconductors.[15,16] To quantify the capacitance more precisely, Radisavljevic and coworkers[17] followed an indirect approach: the capacitance was determined from the carrier density obtained from Hall effect measurements and used in Equation (1). This helps getting more reliable capacitance values than the ones from the parallel-plate capacitor formula, but the gate voltage dependence was not investigated.

In this Letter, we present an easy to implement approach to determine the carrier density and carrier mobility of a MoS₂-LiNbO₃ FET as a function of V_{GS}. For this purpose, we combine standard $I_{SD} - V_{GS}$ with $C - V_{GS}$. The latter probes the carrier system at the chemical potential and allows us to directly derive the carrier density as a function of V_{GS}. All experimental data are found to be in excellent agreement with an analytical model based on a 2D electron system over the entire range of V_{GS}. Most strikingly, we find that for our device, the values of μ_{FE} obtained solely from the $I_{SD} - V_{GS}$ overestimate those obtained taking into account the measured $C - V_{GS}$ by more than a factor of ×4.

The sample studied consists of a 128°Y-rotated, $d = 0.5$ mm thick substrate of black lithium niobate (LiNbO₃₋ₓ), on top of which a layer of MoS₂ has been deposited by chemical vapour deposition.[18,19] We use such samples for investigations of the interaction of surface acoustic waves with MoS₂, as described in Ref. 19. The sample was characterized by

---

a)Electronic mail: wladislaw.michailow@gmx.de
b)Electronic mail: hubert.krenner@physik.uni-augsburg.de

mapping photoluminescence spectroscopy to confirm the millimeter-scale growth of MoS_2. FET devices were fabricated using an established process:[19] the MoS_2 layer has been removed from the sample surface except for two $0.3\,mm \times 6.43\,mm$ stripes. This $A \approx 3.86\,mm^2$ lithographically defined area includes the regions of the highest emission intensity. On top of these stripes, two finger electrodes ($10\,nm$ Ti and $60\,nm$ Au) with a distance of $6.37\,\mu m$ serve as source and drain contacts, contacting the two stripes along their entire $2 \times 0.3\,mm$ width. The gate voltage (V_{GS}) was applied on the sample backside. A schematic of the sample is shown as the inset in Fig. 1. All measurements have been performed under ambient conditions with the device mounted inside a sealed metal chip carrier to exclude any influences of external illumination.

As a first estimate of μ_{FE}, we measured the source-drain current I_{SD} at a fixed source-drain voltage V_{SD} as a function of V_{GS}, as depicted in Fig. 1. For each V_{SD}, a weak hysteresis[14] is resolved as the V_{GS} was scanned $0 \to +40\,V \to -40\,V \to 0\,V$, which is less pronounced than that reported for a different sample in our previous work.[19] The polarity of V_{GS} is chosen such that $V_{GS} > 0$ corresponds to negative charge on the MoS_2 layer. These characteristics directly confirm the accumulation of negative charge on the MoS_2 layer for $V_{GS} > 0$. From these data, we extracted V_{Th} and μ_{FE} using Eq. (1) and the simple parallel-plate capacitor model. The obtained values V_{Th} and μ_{FE} are plotted as a function of V_{SD} as red symbols in Figs. 2(a) and 2(b), respectively. Obviously, both the obtained values and their statistical errors exhibit significant scatter for the different values of V_{SD}. These shortcomings arise from the simple parallel-plate capacitor model and the fact that the V_{GS}-interval, in which the best fit of Eq. (1) is performed, is chosen by eye in the conducting region, so that all other data are neglected. We note that this device shows similar characteristics to that
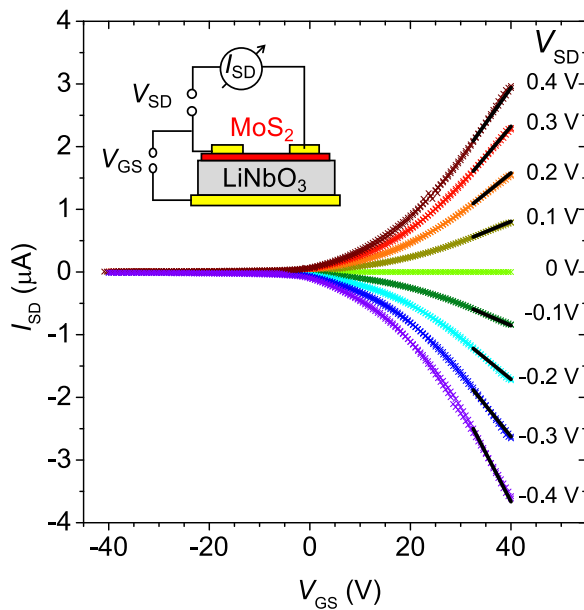
reported in our previous work.[19] In particular, μ_{FE} lies in the same range. In order to improve our method, we directly quantify the capacitance between one contact and the back gate as a function of V_{GS}. V_{GS} is applied as a DC offset gate voltage to the capacitance bridge circuit and modulated with a $1\,kHz$ sine wave by the built-in oscillator. The measured capacitance was corrected for the capacitance of the wires connecting to the sample. In Fig. 3(a), we plot the obtained capacitance of the sample C_{sample} (symbols) as a function of V_{GS}. For large negative V_{GS}, C_{sample} saturates at a constant value of $C_{sample} = 2.06\,pF$. Under these conditions, the MoS_2 layer is completely depleted, and the measured C_{sample} corresponds to that of the metal contacts $C_{contacts}$, which is independent of V_{GS}. As V_{GS} increases, the surrounding MoS_2 2D layer is populated with electrons and the capacitance increases as observed in the data. $C_{sample}(V_{GS})$ can be readily described as an equivalent circuit of $C_{contacts}$ connected in parallel with the V_{GS}-dependent capacitance of the TMD layer $C_{MoS_2}(V_{GS})$, shown as the inset in Fig. 3(a). From $C_{MoS_2}(V_{GS}) = C_{sample}(V_{GS}) - C_{contacts}$, we can directly calculate the electron surface density $n(V_{GS})$ on the MoS_2 layer by a discrete integration. The symbols in Fig. 3(b) are the result obtained from

$$n(V_{GS}) = -\frac{1}{e \cdot A} \cdot \int_{-\infty}^{V_{GS}} C_{MoS_2}(V'_{GS}) dV'_{GS},$$

with e being the elementary charge. The obtained values for $n(V_{GS})$ faithfully reproduce a clear turn-on behavior and linear increase as expected for a FET.

We proceed by developing an analytical model of the V_{GS}-dependent electron density n. The equilibrium electron density can be calculated by integrating the Fermi distribution function $f_{FD}(E) = \left(\exp \frac{(E-\zeta)}{k_B T} + 1 \right)^{-1}$ over the two-dimensional momenta $\vec{p}$

$$n = \frac{g}{A} \cdot \sum_{\vec{p}} f_{FD}(E(\vec{p})) = \frac{2\pi g m^* \cdot k_B T}{h^2} \cdot \ln\left[1 + \exp\left(\frac{\zeta}{k_B T}\right)\right], \quad (2)$$

where $g = 2 \times 2$ is the spin and valley degeneracy for MoS_2, $E(p) = p^2/2m^*$, m^* the electron effective mass, A the area of the monolayer, and h the Planck constant; the energy is counted from the conduction band edge in MoS_2. In the presence of a gate voltage, the chemical potential ζ in (2) should be modified as $\zeta \to \zeta + \delta\zeta(V_{GS})$, where $\delta\zeta(V_{GS})$ is the shift of ζ in MoS_2 due to V_{GS}. We assume that $\delta\zeta(V_{GS})$ is proportional to V_{GS}, i.e., $\delta\zeta(V_{GS}) = \alpha \cdot e \cdot V_{GS}$ and use the following function to fit our experimental data:

$$f(V_{GS}) = a \cdot b \cdot \ln\left[1 + \exp\left(\frac{V_{GS} - V_{Th}}{b}\right)\right], \quad (3)$$

with V_{Th} being a threshold voltage. The result of the best fit of this function to the n derived from the measured capacitance is plotted as the solid line in Fig. 2(b) and shows that this analytical function perfectly follows the experimental data over the entire range of V_{GS}.

The values of the parameters a and b extracted from the fit are $a = 2.73 \times 10^8\,V^{-1}\,cm^{-2}$ and $b = 10.8\,V$. Since

FIG. 1. Measured source-drain current as a function of the applied gate voltage for a set of source-drain voltages V_{SD} tuned from $-0.4\,V$ (violet) to $0.4\,V$ (dark red) in steps of $0.1\,V$. Black lines are tangent fits to the approximately linear region of the curves. Inset: Schematic of experimental setup for measuring transport characteristics with the sample, side view.
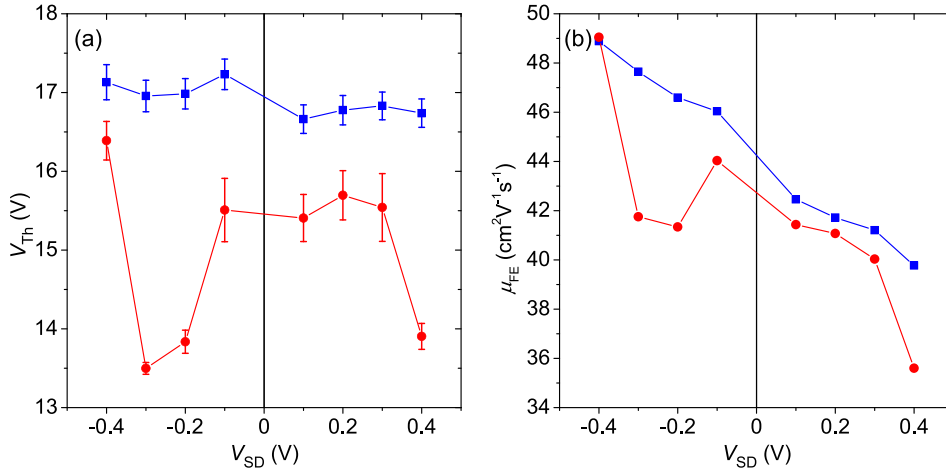
FIG. 2. (a) Threshold voltage V_{Th} and (b) the mobility μ_{FE} as a function of V_{SD}. Red symbols are from linear fits to the linear region of the transport characteristics shown in Fig. 1. Blue symbols are extracted from the best fits of (3) to the data in Fig. 1. The error bars represent the statistical errors of the fit.
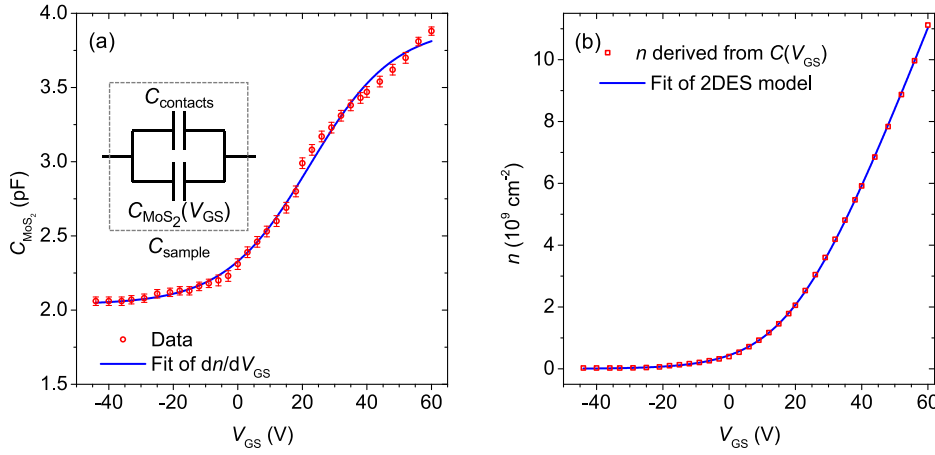

FIG. 3. (a) Measured capacitance (symbols) of the sample as a function of the gate voltage. The error bars represent the statistical error and result of the best fit of function (4) to the data (solid lines). Inset: Equivalent circuit. (b) Electron density (symbols) obtained from the measured capacitance shifted by the constant offset and best fit by function (3) to the data (solid line).

$k_B T/e \approx 26\,\text{mV}$, we get from b the value of $\alpha \approx 2.4 \times 10^{-3}$. Such a small value of $\alpha = \delta\zeta(V_{GS})/eV_{GS}$ suggests that the position of the electrochemical potential in the MoS$_2$–metal contact system is essentially determined by the contacts, where the density of states is substantially larger than that in MoS$_2$. Indeed, in equilibrium (without gate voltage), a small Schottky barrier, $\lesssim 0.1\,\text{eV}$, is typically built up at the metal–TMD interface.[20] Under these conditions, a certain amount of electrons flow into MoS$_2$ from the contacts, so that the density n is inhomogeneous and larger in the near-contact areas than in the areas farther away. A positive V_{GS} increases the electron density in the top metal contact. The additional electrons accumulate at the bottom of the contact in a layer with a thickness corresponding to the Thomas-Fermi screening length, which leads to a small increase of the electrochemical potential $\delta\zeta(V_{GS})$ in the MoS$_2$–metal contact system. Due to the high density of states in the metal, $\delta\zeta(V_{GS})$ is much smaller than $e \cdot U_G$, which yields $\alpha \ll 1$. Due to the growth of $\zeta(V_{GS})$, more electrons flow into MoS$_2$ and larger areas of the 2D semiconductor become well-conducting. This basic physical picture qualitatively agrees with our results.

Comparing Equations (2) and (3), one can see that $a = 2\pi g m^* \cdot e\alpha/h^2$. Using α extracted from b and $m^* \approx 0.45 \times m_e$, 0,[20] one gets $a \approx 9 \times 10^{11}\,\text{V}^{-1}\,\text{cm}^{-2}$. In order to explain the deviation from the fit value, a more accurate model is necessary, which takes into account the concrete contact geometry and coordinate dependence.

An analytical expression for the capacitance can be directly obtained by taking the derivative of Eq. (3). We obtain

$$C(V_{GS}) = (C_\infty - C_{contacts}) \cdot \frac{1}{\exp\left(\dfrac{V_{Th} - V_{GS}}{b}\right)} + C_{contacts},$$

(4)

with C_∞ being the maximum capacitance for $V_{GS} \to \infty$. The result of the best fit of Eq. (4) to the measured capacitance is shown as a solid line in Fig. 3(a), which again faithfully reproduces the experimental data points.

In the next step, we assume that μ_{FE} is independent of V_{GS}. Thus, in the Drude model, $I_{SD}(V_{GS}) \propto n(V_{GS})$ can be fitted using Eq. (3). The results of such best fits for *all* measured $I_{SD}(V_{GS})$ values are plotted as solid lines in Fig. 4(a). Again, the fitted function faithfully reproduces the experimental data, underlining further the 2DES nature of the conducting channel. Furthermore, these obtained fit functions allow us to determine $V_{Th}(V_{SD})$ and $\mu_{FE}(V_{SD})$, using Eq. (1) with $\partial I_{SD}/\partial V_{GS} = a$ as the slope at large V_{GS}, with higher precision. The extracted values for $V_{Th}(V_{SD})$ and $\mu_{FE}(V_{SD})$ are plotted as blue symbols in Figs. 2(a) and 2(b), respectively. Clearly, the scatter of the values derived from the fit results is dramatically reduced. We obtain $\langle V_{Th} \rangle = (17.0 \pm 0.2)\,\text{V}$, which is almost constant over the entire range of V_{SD}. In contrast, $\mu_{FE}(V_{SD})$ exhibits a clear trend to significantly decrease with increasing V_{SD}. The negative slope of the V_{SD}-
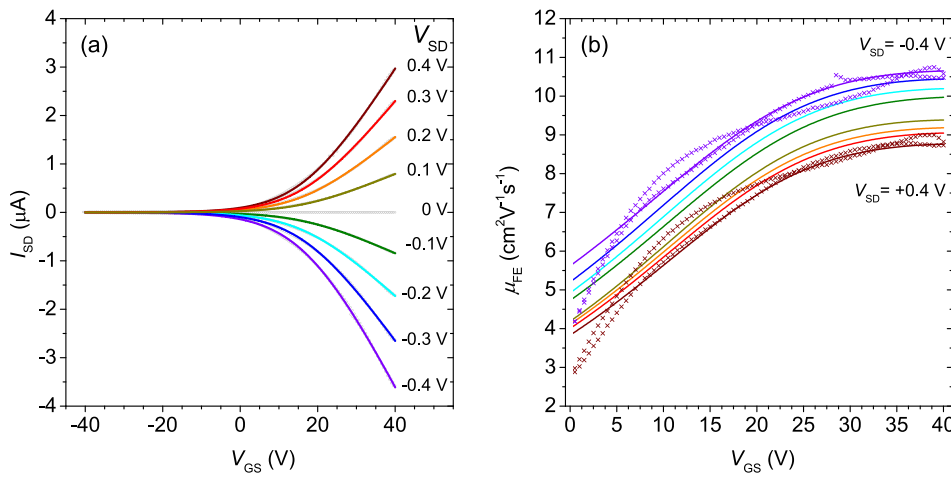
FIG. 4. (a) Best fits (solid lines) of function in (3) to measured $I_{SD}(V_{GS})$ characteristics of Fig. 1 (grey symbols). (b) Field effect mobility μ_{FE} as a function of V_{GS} as obtained from the measured (symbols) and fitted (lines) $I_{SD}(V_{GS})$ and fitted $C(V_{GS})$ data for different values of V_{SD}.

dependence of the mobility has its reason predominantly in hysteresis and drifts of the electrical characteristics. Both effects are commonly observed in such devices.[14,21]

Finally, we turn to carrier mobility and its dependence on the gate voltage, $\mu_{FE}(V_{GS})$. In the Drude model, the conductivity is given by $\sigma = e \cdot n \cdot \mu_{FE}$. Thus, the mobility given by $\mu_{FE}(V_{GS}) = \sigma(V_{GS})/(e \cdot n(V_{GS}))$ can be calculated only from measured data: $\sigma(V_{GS})$ can be derived from the $I_{SD}(V_{GS})$ characteristics [Figs. 1 and 4(a)] and $n(V_{GS})$ from the $C_{MoS_2}(V_{GS})$ data [cf. Fig. 4(b)]. We note that this analysis can be performed for our data only for $V_{GS} \gtrsim 0\,\text{V}$. For negative V_{GS}, both σ and n vanish and any obtained value of $\mu_{FE} \sim \sigma/n$ exhibits a large error. In Fig. 2(b), we plot $\mu_{FE}(V_{GS})$ obtained directly from the measured (symbols) and the fitted (lines) $I_{SD}(V_{GS})$ characteristics for different values of V_{SD} for $V_{GS} > 0\,\text{V}$. Remarkably, the *absolute* value of μ_{FE} shown in Fig. 4(b), which we obtained by including *measured, realistic* capacitance (and thereby n) data, is significantly lower than that obtained from the basic parallel-plate capacitor model [cf. Fig. 2(b)]. It ranges between $\mu_{FE}(V_{GS}) \sim 4$–$10\,\text{cm}^2\,\text{V}^{-1}\,\text{s}^{-1}$ and shows a pronounced increase with increasing V_{GS} (in addition to its global reduction as V_{SD} reduces [cf. Fig. 2(b)]). For $0 < V_{GS} < V_{Th}$, μ_{FE} rapidly increases as the injected electrons screen scattering centers in the channel. Such behavior is well known and has been observed for 2DES in established III–V semiconductor heterostructures.[22,23] For $V_{GS} > V_{Th}$, this trend weakens and μ_{FE} saturates. This saturation behavior can be readily understood considering that the chemical potential ζ is fully shifted into the conduction band. For large positive V_{GS}, the chemical potential lies well above the random potential modulation induced by scattering centers. Thus, any further increase of ζ (i.e. n) does not lead to improved screening and thus increased μ_{FE}.

In summary, we demonstrated that combined electrical transport ($I_{SD} - V_{GS}$) and capacitance ($C - V_{GS}$) spectroscopy allows us to determine the field-effect mobility μ_{FE} and threshold voltage V_{Th} of a TMD based FET with significantly higher precision than the commonly applied basic parallel-plate capacitor model. We performed a three step analysis on model data of a MoS_2-$LiNbO_3$ FET device starting with the basic parallel-plate capacitor model. For our device, the V_{GS}-dependent I_{SD}, n, and C are in excellent agreement with an analytical model of an ideal 2DES over the *entire range of* V_{GS}. This is in strong contrast to the basic parallel-plate capacitor model in which only data in a small, subjectively chosen interval of the $I_{SD} - V_{GS}$-characteristics are considered. The statistical errors of μ_{FE} and V_{Th} can be significantly reduced by fitting and evaluating the $I_{SD} - V_{GS}$-characteristics using our 2DES model as now the full data range is included. Finally, by including the full $C - V_{GS}$-characteristics and the derived carrier density n, we are able to obtain the V_{GS}-dependent μ_{FE}. For our device, we nicely observe a pronounced increase of μ_{FE} at V_{Th} due to the onset of efficient electrostatic screening. Most strikingly, the absolute value of μ_{FE} obtained this way is significantly lower than that obtained from the basic parallel-plate capacitor model. Our full method is especially important for back-gated 2D material-based FETs. For such devices, the distance between the 2D carrier system and the gate electrode is large compared to the lateral dimensions of typical flakes. It enables (i) the direct confirmation of the 2DES-like character of the FET operation and derives (ii) more accurate, realistic, and (iii) V_{GS}-dependent values μ_{FE}. Moreover, it does not require a magnetic field as the mobility determination via the Hall effect, thus making it suitable for setups without magnets and for samples with low mobilities, for which the Hall angle is small.

[1]K. S. Novoselov, A. K. Geim, S. V. Morozov, D. Jiang, Y. Zhang, S. V. Dubonos, I. V. Grigorieva, and A. A. Firsov, "Electric field effect in atomically thin carbon films," Science **306**, 666–669 (2004).
[2]K. S. Novoselov, A. K. Geim, S. V. Morozov, D. Jiang, M. I. Katsnelson, I. V. Grigorieva, S. V. Dubonos, and A. A. Firsov, "Two-dimensional gas of massless Dirac fermions in graphene," Nature **438**, 197–200 (2005).

[3]Y. Zhang, Y.-W. Tan, H. L. Stormer, and P. Kim, "Experimental observation of the quantum Hall effect and Berry's phase in graphene," Nature **438**, 201–204 (2005).

[4]K. S. Novoselov, D. Jiang, F. Schedin, T. J. Booth, V. V. Khotkevich, S. V. Morozov, and A. K. Geim, "Two-dimensional atomic crystals," Proc. Natl. Acad. Sci. U. S. A. **102**, 10451–10453 (2005).

[5]A. C. Ferrari, F. Bonaccorso, V. Fal'ko, K. S. Novoselov, S. Roche, P. Boggild, S. Borini, F. H. L. Koppens, V. Palermo, N. Pugno, J. A. Garrido, R. Sordan, A. Bianco, L. Ballerini, M. Prato, E. Lidorikis, J. Kivioja, C. Marinelli, T. Ryhanen, A. Morpurgo, J. N. Coleman, V. Nicolosi, L. Colombo, A. Fert, M. Garcia-Hernandez, A. Bachtold, G. F. Schneider, F. Guinea, C. Dekker, M. Barbone, Z. Sun, C. Galiotis, A. N. Grigorenko, G. Konstantatos, A. Kis, M. Katsnelson, L. Vandersypen, A. Loiseau, V. Morandi, D. Neumaier, E. Treossi, V. Pellegrini, M. Polini, A. Tredicucci, G. M. Williams, B. Hee Hong, J.-H. Ahn, J. Min Kim, H. Zirath, B. J. van Wees, H. van der Zant, L. Occhipinti, A. Di Matteo, I. A. Kinloch, T. Seyller, E. Quesnel, X. Feng, K. Teo, N. Rupesinghe, P. Hakonen, S. R. T. Neil, Q. Tannock, T. Lofwander, and J. Kinaret, "Science and technology roadmap for graphene, related two-dimensional crystals, and hybrid systems," Nanoscale **7**, 4598–4810 (2015).

[6]Q. H. Wang, K. Kalantar-Zadeh, A. Kis, J. N. Coleman, and M. S. Strano, "Electronics and optoelectronics of two-dimensional transition metal dichalcogenides," Nat. Nanotechnol. **7**, 699–712 (2012).

[7]K. F. Mak, C. Lee, J. Hone, J. Shan, and T. F. Heinz, "Atomically thin MoS_2: A new direct-gap semiconductor," Phys. Rev. Lett. **105**, 136805 (2010).

[8]A. Splendiani, L. Sun, Y. Zhang, T. Li, J. Kim, C.-Y. Chim, G. Galli, and F. Wang, "Emerging photoluminescence in monolayer MoS_2," Nano Lett. **10**, 1271–1275 (2010).

[9]O. Lopez-Sanchez, D. Lembke, M. Kayci, A. Radenovic, and A. Kis, "Ultrasensitive photodetectors based on monolayer MoS_2," Nat. Nanotechnol. **8**, 497–501 (2013).

[10]Z. Sun, A. Martinez, and F. Wang, "Optical modulators with 2D layered materials," Nat. Photonics **10**, 227–238 (2016).

[11]B. Radisavljevic, A. Radenovic, J. Brivio, V. Giacometti, and A. Kis, "Single-layer MoS_2 transistors," Nat. Nanotechnol. **6**, 147–150 (2011).

[12]B. Radisavljevic, M. B. Whitwick, and A. Kis, "Integrated circuits and logic operations based on single-layer MoS_2," ACS Nano **5**, 9934–9938 (2011).

[13]G. Fiori, F. Bonaccorso, G. Iannaccone, T. Palacios, D. Neumaier, A. Seabaugh, S. K. Banerjee, and L. Colombo, "Electronics based on two-dimensional materials," Nat. Nanotechnol. **9**, 768–779 (2014).

[14]D. J. Late, B. Liu, H. S. S. R. Matte, V. P. Dravid, and C. N. R. Rao, "Hysteresis in single-layer MoS_2 field effect transistors," ACS Nano **6**, 5635–5641 (2012).

[15]M. S. Fuhrer and J. Hone, "Measurement of mobility in dual-gated MoS_2 transistors," Nat. Nanotechnol. **8**, 146–147 (2013).

[16]B. Radisavljevic and A. Kis, "Reply to 'Measurement of mobility in dual-gated MoS_2 transistors'," Nat. Nanotechnol. **8**, 147–148 (2013).

[17]B. Radisavljevic and A. Kis, "Mobility engineering and a metal–insulator transition in monolayer MoS_2," Nat. Mater. **12**, 815–820 (2013).

[18]A. Nguyen, P. Sharma, T. Scott, E. Preciado, V. Klee, D. Sun, I.-H. D. Lu, D. Barroso, S. Kim, V. Y. Shur, A. R. Akhmatkhanov, A. Gruverman, L. Bartels, and P. A. Dowben, "Toward ferroelectric control of monolayer MoS_2," Nano Lett. **15**, 3364–3369 (2015).

[19]E. Preciado, F. J. R. Schülein, A. E. Nguyen, D. Barroso, M. Isarraraz, G. von Son, I.-H. Lu, W. Michailow, B. Möller, V. Klee, J. Mann, A. Wixforth, L. Bartels, and H. J. Krenner, "Scalable fabrication of a hybrid field-effect and acousto-electric device by direct growth of monolayer MoS_2/$LiNbO_3$," Nat. Commun. **6**, 8593 (2015).

[20]Y. Yoon, K. Ganapathi, and S. Salahuddin, "How good can monolayer MoS_2 transistors be?," Nano Lett. **11**, 3768–3773 (2011).

[21]Y. Y. Illarionov, G. Rzepa, M. Waltl, T. Knobloch, A. Grill, M. M. Furchi, T. Mueller, and T. Grasser, "The role of charge trapping in MoS_2/SiO_2 and MoS_2/hBN field-effect transistors," 2D Mater. **3**, 035004 (2016).

[22]M. Shayegan, V. J. Goldman, C. Jiang, T. Sajoto, and M. Santos, "Growth of low-density two-dimensional electron system with very high mobility by molecular beam epitaxy," Appl. Phys. Lett. **52**, 1086 (1988).

[23]L. Pfeiffer, K. W. West, H. L. Stormer, and K. W. Baldwin, "Electron mobilities exceeding $10^7 cm^2/V$ sin modulation-doped GaAs," Appl. Phys. Lett. **55**, 1888 (1989).